

This is an Open Access document downloaded from ORCA, Cardiff University's institutional repository: <https://orca.cardiff.ac.uk/id/eprint/152422/>

This is the author's version of a work that was submitted to / accepted for publication.

Citation for final published version:

Lü, Hanghang, Zhu, Jianrong, Chen, Qing, Li, Ming, Pan, Shunqi and Chen, Shenliang 2023. Impact of estuarine reclamation projects on saltwater intrusion and freshwater resource. *Journal of Oceanology and Limnology* 41 , pp. 38-56. 10.1007/s00343-021-1246-z

Publishers page: <http://dx.doi.org/10.1007/s00343-021-1246-z>

Please note:

Changes made as a result of publishing processes such as copy-editing, formatting and page numbers may not be reflected in this version. For the definitive version of this publication, please refer to the published source. You are advised to consult the publisher's version if you wish to cite this paper.

This version is being made available in accordance with publisher policies. See <http://orca.cf.ac.uk/policies.html> for usage policies. Copyright and moral rights for publications made available in ORCA are retained by the copyright holders.



# Impacts of estuarine reclamation projects on saltwater intrusion and freshwater resources

LYU Hanghang<sup>1</sup>, ZHU Jianrong<sup>2</sup> \*\*, CHEN Qing<sup>2</sup>, LI Ming<sup>3</sup>, PAN Shunqi<sup>4</sup>, CHEN Shenliang<sup>2</sup>

<sup>1</sup> CCCC National Engineering Research Center of Dredging Technology and Equipment Co., Ltd., Shanghai, 201208, PR China

<sup>2</sup> State Key Laboratory of Estuarine and Coastal Research, East China Normal University, Shanghai, 200062, PR China

<sup>3</sup> Civil Engineering and Industrial Design, School of Engineering, Liverpool University, Liverpool L69 3GH, UK

<sup>4</sup> Hydro-environmental Research Centre, School of Engineering, Cardiff University, Cardiff CF24 3AA, UK

**Abstract** Estuarine projects can change local topography and influence water transport and saltwater intrusion. The Yangtze River Estuary is a multichannel estuary, and four major reclamation projects have taken place in the Yangtze River Estuary in recent years: the Xincun Shoal reclamation project (RP-XCS), the Qingcao Shoal reclamation project (RP-QCS), the Eastern Hengsha Shoal reclamation project (RP-EHS), and the Nanhui Shoal reclamation project (RP-NHS). The effects of the four reclamation projects and each individual project on the saltwater intrusion and water resources in the Yangtze River Estuary were simulated by a 3D numerical model. The results of this study show that for a multichannel estuary, local reclamation projects change the local topography and water diversion ratio (WDR) between channels and influence water and salt transport and freshwater utilization in the estuary. During spring tide, under the cumulative effect of the four reclamation projects, the salinity decreases by approximately 0.5 in the upper reaches of the North Branch and increases by 0.5-1.0 in the middle and lower reaches of the North Branch. In the North Channel, the salinity decreases by approximately 0.5. In the North Passage, the salinity increases by 0.5-1.0. In the South Passage, the salinity increases by approximately 0.5 in the upper reaches and decreases by 0.2-0.5 on the north side of the middle and lower reaches. During neap tide, the cumulative effects of the four reclamation projects and the individual projects are similar to those during spring tide, but there are some differences. The effects of an individual reclamation project on WDR and saltwater intrusion during spring and neap tides are simulated and analyzed in detail. The cumulative effect of the four reclamation projects favors freshwater usage in the Yangtze River Estuary.

**Keywords:** reclamation projects; saltwater intrusion; freshwater resources; numerical model; Yangtze River Estuary

## 1 INTRODUCTION

Estuaries are located throughout the world and are often economically developed, populated regions (Chua 1993; Shi et al., 2001). Estuarine areas tend to be under pressure from population growth and land scarcity. Therefore, many reclamation projects have been implemented worldwide in estuaries undergoing rapid economic development and an increasing population. Examples include the San Francisco Estuary (Nichols et al., 1986),

31 Ems Estuary (Van Maren et al., 2016), Nakdong Estuary (Doornbos et al., 1986), Sydney Estuary (Birch et al.,  
32 2009), Rhine and Maas Estuary (Kuijpers 1995) and Tolka Estuary (Buggy and Tobin, 2006). China has been  
33 implementing reclamation projects in coastal sea areas since the 1950s (Wang et al., 2014). With the rapid  
34 expansion of China's coastal economy, land demand has sharply increased in recent decades. The total  
35 reclamation area in China reached 13,380 km<sup>2</sup> from 1950 to 2008 (Fu et al., 2010), and an additional 2,469 km<sup>2</sup> of  
36 reclamation projects are planned for implementation between 2012 and 2020 (Wang et al., 2014).

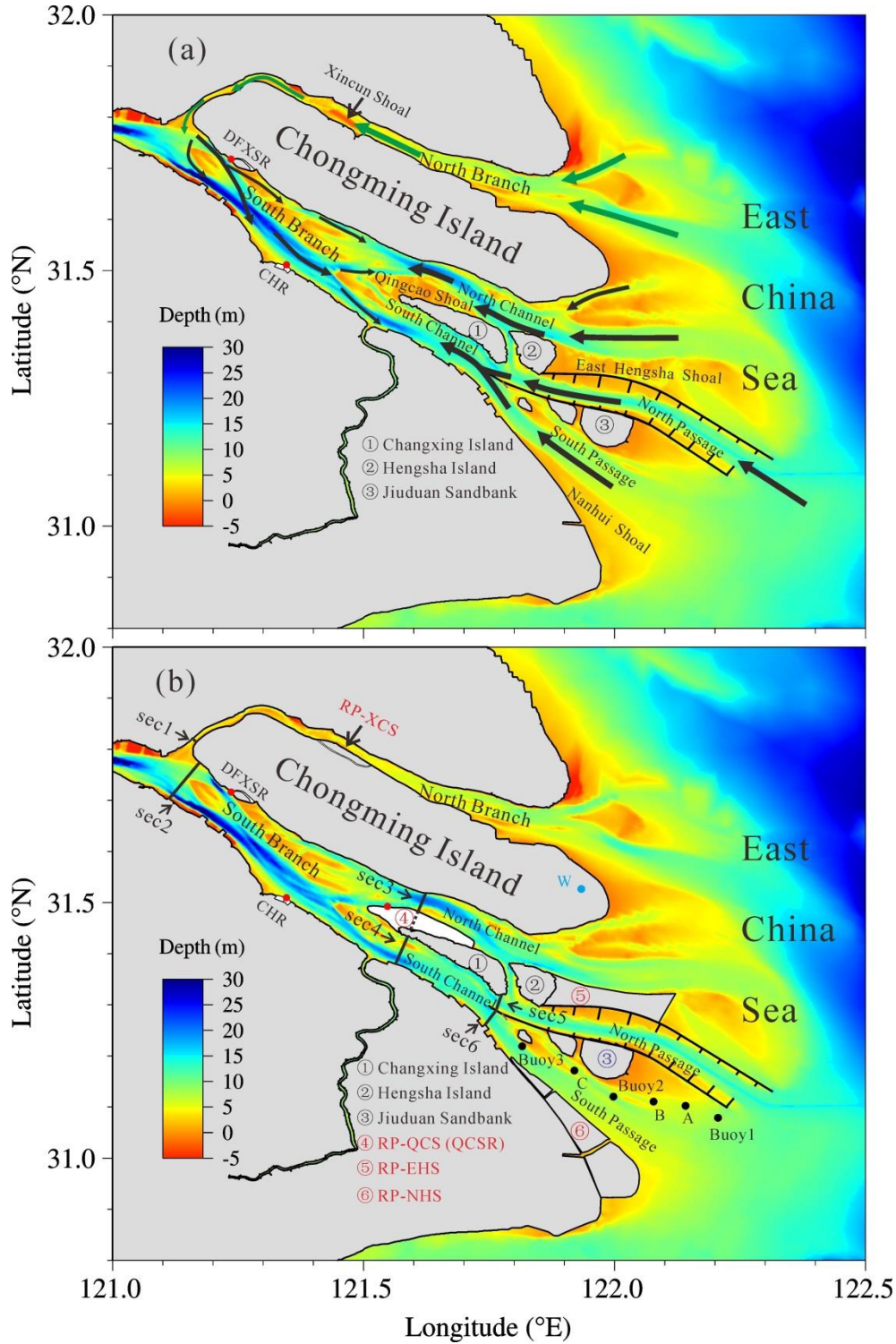
37 The Yangtze River is one of the largest rivers in the world. Shanghai, located near the Yangtze River Estuary  
38 and the so-called 'Golden Coast', with 24 million residents, is China's largest city (Ma et al., 2018; Shi et al.,  
39 2001). With economic and industrial expansion and population growth, many reclamation projects have been  
40 implemented in the Yangtze River Estuary in recent years. The major reclamation projects are shown in Fig.1 and  
41 include the Xincun Shoal reclamation project (RP-XCS), the Qingcao Shoal reclamation project (RP-QCS), the  
42 Eastern Hengsha Shoal reclamation project (RP-EHS), and the Nanhui Shoal reclamation project (RP-NHS). The  
43 RP-XCS was completed in 2012 and blocked the southern channel of the Xincun Shoal in the North Branch,  
44 resulting in an artificial change in river topography. The RP-QCS began on June 5, 2007, and was completed in  
45 October 2010. The main accomplishment of this project was the construction of the Qingcaosha Reservoir  
46 (QCSR), which is located at the bifurcation of the North Channel and South Channel. The RP-EHS is located  
47 between the North Channel and the North Passage and started in December 2003. This reclamation project was  
48 constructed in stages and extends the length of the North Channel. The Nanhui Shoal is located on the south side  
49 of the South Passage. Construction of the RP-NHS started in March 2013 and is still ongoing.

50 Previous studies indicated that estuarine reclamation projects can change the local topography and will affect  
51 hydrodynamic processes and saltwater intrusion. For example, Han et al. (2001) found that a large-scale reservoir  
52 and river reclamation would decrease saltwater intrusion in the Qiantang Estuary. Manda and Matsuoka (2006)  
53 found that the reclamation project in the innermost part of Ariake Sound could cause the tidal currents to decrease  
54 by more than 10% over a large area. Song et al. (2013) found that the reclamation project on the west coast of  
55 Korea could result in an increase in tidal amplitude. Xu (2014) found that a large-scale reclamation project would  
56 have some effects on saltwater intrusion in the Oujiang River Estuary. Andrews et al. (2017) found that  
57 reclamation and other anthropogenic projects in the San Francisco Estuary had effects on saltwater intrusion due  
58 to changes in estuary geometry.

59 The impacts of each of the reclamation projects mentioned above, such as the RP-XCS, RP-NHS and  
60 RP-EHS, on saltwater intrusion in the Yangtze River Estuary were examined. For example, the RP-XCS  
61 weakened the saltwater spillover (SSO), which favors the utilization of freshwater in the South Branch (Chen and

62 Zhu, 2014). The RP-NHS could weaken the salinity front in the South Passage (Li and Zhu, 2015). The RP-EHS  
 63 enhanced saltwater intrusion in the South Channel, North Passage and South Passage and weakened saltwater  
 64 intrusion in the North Channel (Lyu and Zhu, 2019). However, the combined influences of the RP-XCS, RP-QCS,  
 65 RP-EHS and RP-NHS have not been examined. The aim of this study is to address this issue.

66



67

68 Fig.1 River regime of the Yangtze River Estuary before (a) and after (b) the reclamation project and the pathways of  
 69 saltwater intrusion (arrows). The four reclamation projects are labeled. Red dots are the locations of water intake for the

three reservoirs, and the cross-channel sections are marked by black lines. Black dots indicate the locations of three ship measurement sites A, B, C and three buoy measurement sites Buoy 1, Buoy 2 and Buoy 3 in March 2018 in the South Passage; W is the location of the Chongming Weather Station

## 2 MATERIALS AND METHODS

### 2.1 Study area

The Yangtze River Estuary, located from Shanghai to the offshore of southern Jiangsu Province in China between 30.8°N–32°N and 121°E–122.5°E, is a funnel-shaped estuary (Fig.1). The Yangtze River Estuary is 90 km wide and is a typical estuary with multiple bifurcations (Fig.1). First, the estuary is bifurcated into the South Branch and North Branch. Second, the lower South Branch is divided by Changxing Island into the South Channel and the North Channel. Finally, the South Channel is bifurcated into the South Passage and the North Passage by Jiuduansha Island. The grooves and tidal flats alternate and have developed in the different channels. As a whole, the depth of the Yangtze River Estuary gradually deepens seaward. Most tidal flats are in the North Branch and the mouth of the Yangtze River Estuary. The average depth of the North Branch is very shallow, especially in the upper reaches of the North Branch, which is only 2-4 m deep. The average depth of the North Branch is 5-30 m (Chen et al., 2019). Therefore, the South Branch is the main channel discharging runoff. The Yangtze River Estuary is a mesotidal estuary (Shen et al., 2003). The tides in the Yangtze River Estuary exhibit semidiurnal, diurnal, and fortnightly spring–neap cycles (Zhu, et al., 2015).

In the Yangtze River Estuary, longitudinal and lateral saltwater intrusions coexist, and both saltwater intrusions can affect the temporal variation and spatial distribution of salinity (Fig.1a) (Li et al., 2014; Lyu and Zhu, 2018; Qiu et al., 2012; Wu et al., 2006; Zhu et al., 2015). There are four outlets (the North Branch, North Channel, North Passage and South Passage) into the sea in the Yangtze River Estuary. In the North Channel, North Passage and South Passage, the saltwater from the sea mainly intrudes along the longitudinal direction, consistent with most estuaries. The particular lateral saltwater intrusion in the Yangtze River Estuary is saltwater spillover (SSO) from the North Branch into the South Branch. From the 1950s to 2000s, natural forces and human activities severely narrowed the North Branch. Consequently, the upper reaches of the North Branch have become almost perpendicular to the South Branch, while the lower reaches have become funnel shaped. The evolution of topography led to a reduction in runoff entering the North Branch, especially during the dry season, and also caused the tidal range in the North Branch to be greater than that in the South Branch. Strong tidal forcing in the North Branch induces considerable subtidal circulation, resulting in a net landward flow when river discharge is

low during spring tide (Wu et al., 2006). This residual transport forms the SSO, which is the most characteristic type of saltwater intrusion in the estuary (Li et al., 2014; Lyu and Zhu, 2018; Wu et al., 2006; Xue et al., 2009). Saltwater intrusion will cause estuarine stratification and affect estuarine circulation (Geyer, 1993; Simpson et al., 1990). The degree of mixing in the Yangtze River Estuary differs among the different channels. In the North Branch, the water is well mixed. The diversion ratio of river discharge in the North Branch is very small (approximately 1%) owing to the special river regime (the North Branch is almost perpendicular to the main channel and is very shallow). Additionally, the shape of the North Branch is similar to that of the mouth of a horn, so the tidal range is greater. Therefore, vertical mixing is strong in the North Branch. In the South Branch, especially near the mouth, the salinity is partially mixed in spring tide and weakly mixed in neap tide (a salt wedge appears). Additionally, the lateral intrusion is stronger on the north side than on the south side of a channel due to the Coriolis force (Li et al., 2014; Lyu and Zhu, 2018). Together with the SSO, the landward saltwater intrusion along the North Channel threatens the water intake of the reservoirs, i.e., the QCSR, Dongfengxisha Reservoir (DFXSR) and Chenhang Reservoir (CHR). The QCSR is the largest tidal estuary freshwater reservoir worldwide. More than 70% of the freshwater for Shanghai is supplied by the QCSR, but the QCSR is frequently influenced by saltwater intrusion during the dry season (Chen et al., 2019; Wang and Zhu, 2015; Zhu et al., 2010). The reservoirs cannot receive water from the Yangtze River Estuary when the salinity exceeds 0.45, which is the salinity standard for drinking water.

## 2.2 Model configuration

A 3D numerical model (ECOM-si) was adopted in this study. This model has been applied and developed continuously by many researchers (Blumberg, 1994; Chen et al. 2001; Wu and Zhu, 2010; Zheng et al., 2003; Zheng et al., 2004; Zhu, 2003). The Mellor-Yamada level 2.5 turbulence closure module (Mellor and Yamada 1982) with stability parameters from Kantha and Clayson (1994) was included. In this study, the domain of the model covers the Yangtze River Estuary and its adjacent sea (from 117.5 to 125 °E longitude and 27.5 to 33.7 °N latitude) (Fig.2). The model grid was composed of  $337 \times 225$  cells horizontally and 10 uniform  $\sigma$  levels vertically. The resolutions of the model varied from 100 m to 10 km around the Yangtze River Estuary. The model can simulate tidal currents, estuarine circulation, and the spatial and temporal distributions of salinity with little sacrifice in terms of run time. The Datong station recorded daily river discharge, which can be used in the model as the river boundary condition. In this study, the mean discharge during the dry season ( $11,500 \text{ m}^3/\text{s}$ ) was adopted in all experiments. The open sea boundary was driven by 16 astronomical constituents:  $M_2$ ,  $S_2$ ,  $N_2$ ,  $K_2$ ,  $K_1$ ,  $O_1$ ,  $P_1$ ,  $Q_1$ ,  $MU_2$ ,  $NU_2$ ,  $T_2$ ,  $L_2$ ,  $2N_2$ ,  $J_1$ ,  $M_1$ , and  $OO_1$ . The initial salinity distribution around the Yangtze River Estuary was derived from the Ocean Atlas in the Huanghai Sea and East China Sea (Hydrology) (Editorial Board for Marine

131 Atlas 1992). The semimonthly mean wind data of ten years from the NECP (National Centers for Environmental  
132 Prediction) with a resolution of  $0.25^{\circ} \times 0.25^{\circ}$  were used. Ecom-si adopted the HSIMT-TVD advection scheme to  
133 solve the transport equations developed by Wu and Zhu (2010). This scheme features third-order accuracy and can  
134 prevent numerical oscillations from exacerbating the calculation error. The model adopted the implicit  
135 time-stepping method, which could break the limits of the Courant-Friedrichs-Lewy (CFL) stability criterion (Lax  
136 and Wendroff, 1962) for the external mode at the cost of solving an elliptic system. The density in the model is  
137 calculated by using the parameterized formula of Fofonoff and Millard (Fofonoff and Millard, 1983) based on the  
138 salinity, temperature and pressure at the current time. The temperature in the Ecom-si was set at 10°C. The  
139 hydrodynamic and salinity formulas are solved at the same time step. The integrated time step was set to 40 s for  
140 all experiments. The concrete calculation process of Ecom-si is shown in Fig.2. More detail about the numerical  
141 model setup can be found in Wu et al. (2011).

142



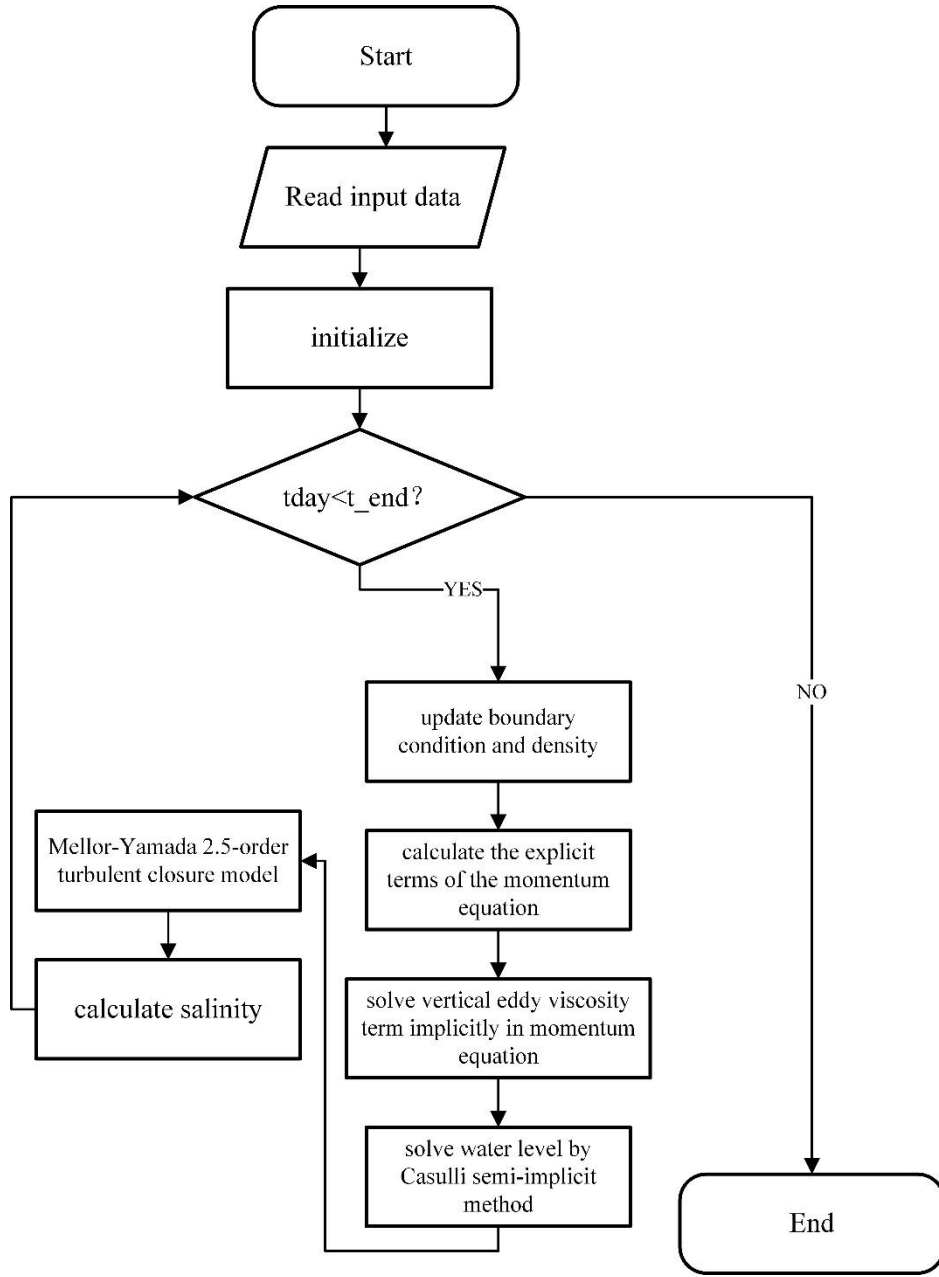


**Fig.2 The flow chart of ECOM-si computational process**

To describe the water and salt transport, the residual unit width water flux (RUWF) and the residual unit width salt flux (RUSF) are defined as follows:

$$\vec{F} = \int_{h2}^{h1} \vec{V} dz$$

$$RUWF = \frac{1}{T} \int_0^T \vec{F} dt$$

$$RUSF = \frac{1}{T} \int_0^T \vec{F} s dt$$

where  $\vec{F}$  is the instantaneous rate of water transport per unit width through a layer and  $h1$  and  $h2$  are the upper and lower bounds of the water layer, respectively.  $\vec{V}$  is the current vector in the specific layer,  $H$  is the total water depth, and  $Z$  is the depth of the relative  $\sigma$  layer bound.  $T$  is the time period (which equals one or



several tidal cycles; in this study, it equals six semidiurnal tidal cycles) used as an averaging time window to remove the tidal signals.  $s$  is salinity.

Additionally, the residual transection water flux (NTWF) is determined to calculate the WDR between channels (transection locations labeled in Fig.1) as follows:

$$NTWF = \frac{1}{T} \int_0^T \int_{-H(x,y)}^{\zeta} \int_0^L \vec{V}_n(x, y, z, t) dl dz dt$$

where  $\zeta$  is the elevation,  $H(x, y)$  is the depth,  $L$  is the width of the transect, and  $\vec{V}_n(x, y, z, t)$  is the velocity component vertical to the transect.

The model calculation period starts on December 1, 2014, and ends at the end of February 2015, and the calculation results in February are analyzed and compared. The river discharges in December, January and February are set by the average since 1950, as measured by the Datong hydrological station, and these discharges are 13,600, 11,100 and 12,000 m<sup>3</sup>/s, respectively. Six numerical experiments are conducted for contrastive analysis (as shown in Table 1): Experiment 0 (Exp 0) is the control experiment, which is designed to simulate the saltwater intrusion pattern before the four reclamation projects (Fig.3a). Experiment 1 (Exp 1) considers the four projects (Fig.3b). Experiment 2 (Exp 2) only considers the RP-XCS (Fig.3c), Experiment 3 (Exp 3) only considers the RP-QCS (Fig.3d), Experiment 4 (Exp 4) only considers the RP-EHS (Fig.3e), and Experiment 5 (Exp 5) only considers the RP-NHS (Fig.3f).

**Table 1 Different numerical experimental settings for consideration of the reclamation projects**

	Exp0	Exp1	Exp2	Exp3	Exp4	Exp5
RP-XCS		√	√			
RP-QCS		√		√		
RP-EHS		√			√	
RP-NHS		√				√

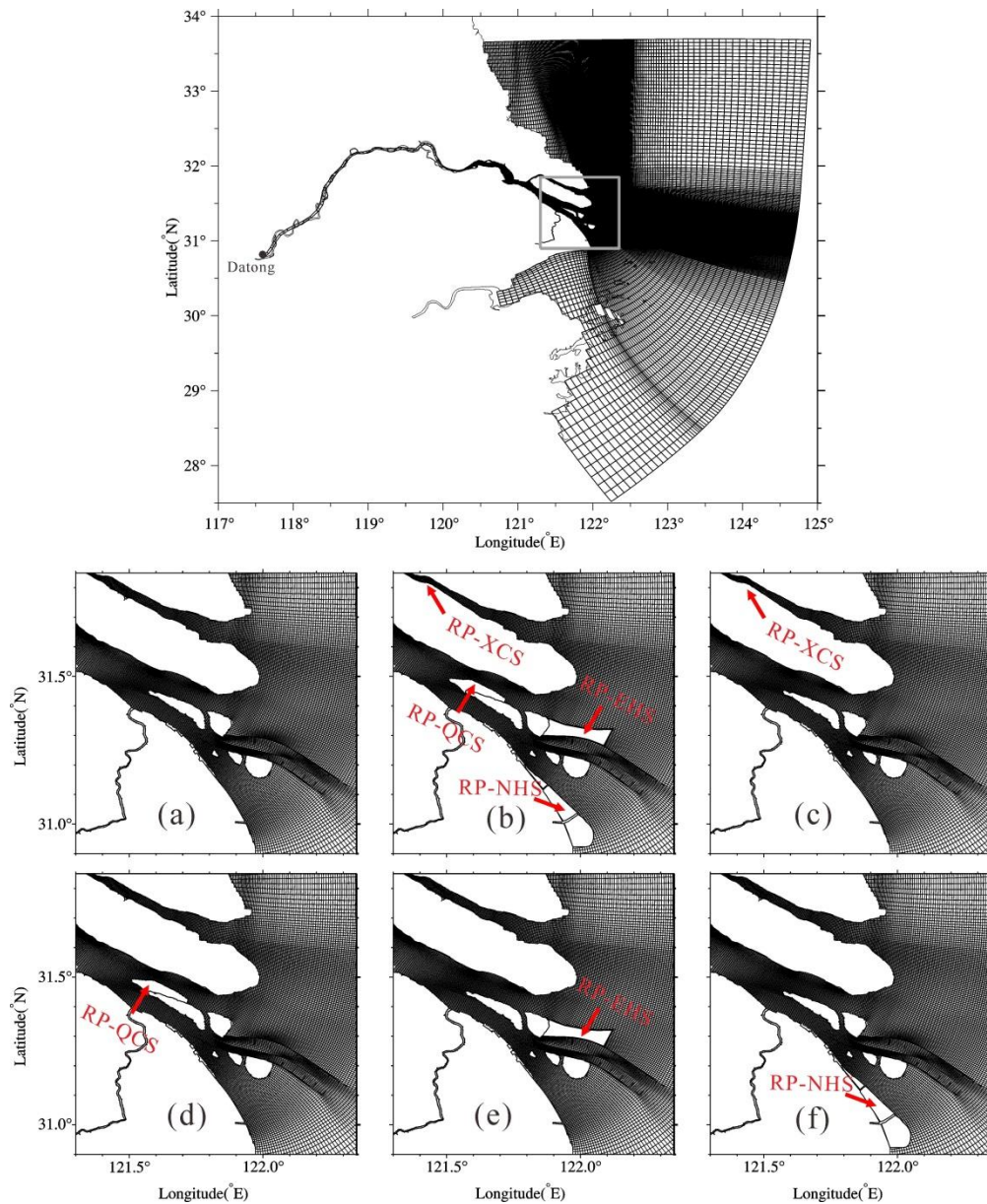


**Fig.3 Numerical model domain and grids. Enlarged views are the different model grids used in the six experiments. (a) No reclamation projects; (b) the four reclamation projects combined; (c) only the RP-XCS; (d) only the RP-QCS; (e) only the RP-EHS; and (f) only the RP-NHS**

### 2.3 Model validation

The model has been extensively validated in the Yangtze River Estuary (Li et al., 2010; Li et al., 2012; Li et al., 2014; Lyu and Zhu, 2018; Qiu and Zhu, 2013; Qiu and Zhu, 2015). In this paper, the measured data in the South Passage from 9 to 19 in March 2018 were used to validate the model (three buoy sites and three ship sites shown in Fig.1b).

The measured river discharge data recorded by the Datong hydrological station (location as shown in Fig.3) and wind data recorded by the Chongming weather station (W, blue solid circles in Fig.1) were adopted to validate the model. The correlation coefficient (CC), root mean square error (RMSE), and skill score (SS, Wilmott, 1981)

183 were used to quantify the validation as follows:

$$184 \quad CC = \frac{\sum (X_{\text{mod}} - \bar{X}_{\text{mod}})(X_{\text{obs}} - \bar{X}_{\text{obs}})}{[\sum (X_{\text{mod}} - \bar{X}_{\text{mod}})^2 \sum (X_{\text{obs}} - \bar{X}_{\text{obs}})^2]^{1/2}}$$

$$185 \quad RMSE = \sqrt{\frac{\sum (X_{\text{mod}} - X_{\text{obs}})^2}{N}}$$

$$186 \quad SS = 1 - \frac{\sum |X_{\text{mod}} - X_{\text{obs}}|^2}{\sum (|X_{\text{mod}} - \bar{X}_{\text{obs}}| + |X_{\text{obs}} - \bar{X}_{\text{obs}}|)^2}$$

187 where  $X_{\text{mod}}$  is the simulated data,  $X_{\text{obs}}$  is the observed data, and  $\bar{X}$  is the mean value. The value range of  
 188 SS is 0-1. When the SS is closer to 1, the agreement between the simulation results and observations is better. Due  
 189 to space limitations, only the comparison results of the simulation and observations at Site B and Buoy 2 are  
 190 selected and shown in Fig.4 and Fig.5. The assessment indicator scores of simulated water velocity and salinity  
 191 are listed in Table 2 and Table 3, respectively. Comparing the simulated and observed data reveals that the model  
 192 can successfully simulate the variation processes of current and salinity.

193

194 **Table 2 The assessment indicator scores for comparison of simulated and observed water velocities at the surface and bottom**  
 195 **layers at the measured sites**

	Sites	RMSE/(m/s)	CC	SS
Surface layer	Buoy 1	0.3	0.7	0.8
	Buoy 2	0.3	0.9	0.9
	Buoy 3	0.2	0.9	0.9
	A	0.4	0.6	0.8
	B	0.2	0.9	0.9
	C	0.3	0.8	0.9
Bottom layer	Buoy 1	0.1	0.8	0.9
	Buoy 2	0.1	0.8	0.9
	Buoy 3	0.1	0.8	0.9
	A	0.2	0.5	0.7
	B	0.2	0.8	0.9
	C	0.2	0.7	0.8

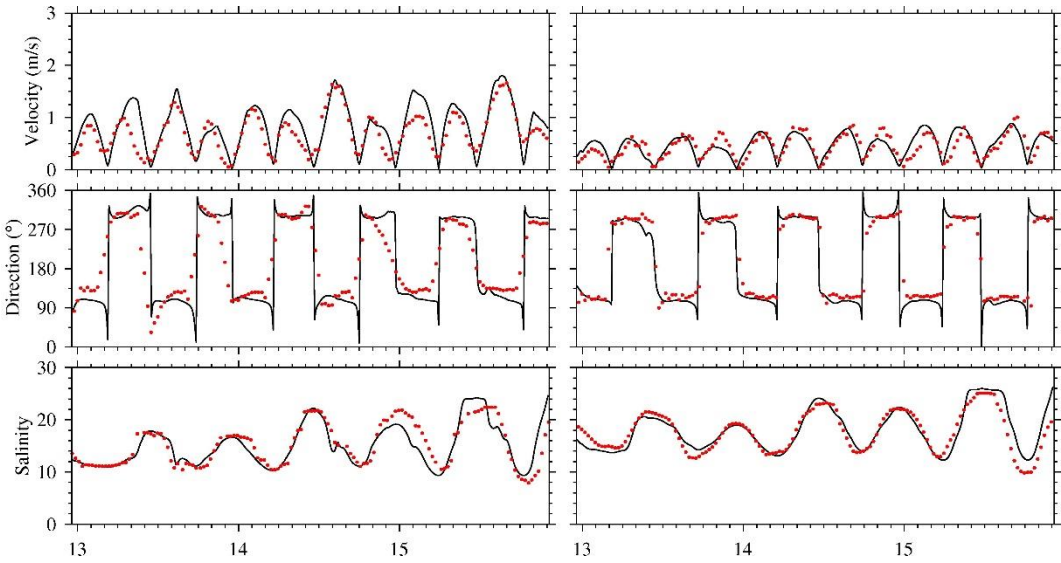
196

197

198 **Table 3 The assessment indicator scores for comparison of simulated and observed salinities at the surface and bottom layers**  
199 **at the measured sites**

	Sites	RMSE	CC	SS
Surface layer	Buoy 1	2.3	0.9	0.9
	Buoy 2	1.7	0.9	1.0
	Buoy 3	0.4	0.8	0.9
	A	1.9	0.7	0.9
	B	2.5	0.9	0.9
	C	2.2	0.7	0.8
Bottom layer	Buoy 1	1.3	0.9	0.9
	Buoy 2	/	/	/
	Buoy 3	0.3	0.9	1.0
	A	2.1	0.7	0.8
	B	1.6	0.9	1.0
	C	1.3	0.9	0.9

200



201

202 **Fig.4 Temporal variation in water velocity, direction and salinity in the neap tide following moderate tide at the surface layer**  
203 **(left) and bottom layer (right) at ship-measured site B. Red dots: measured values; black lines: simulated values**

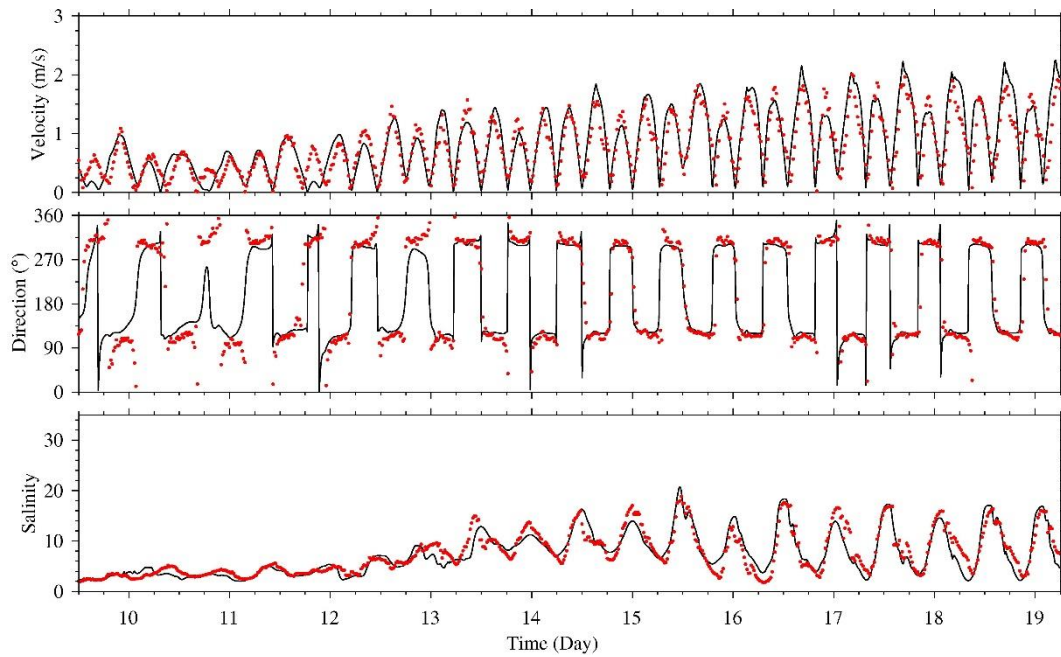


**Fig.5 Temporal variations in water velocity, direction and salinity at the surface layer at buoy-measured site Buoy 2**

### 3 RESULTS AND DISCUSSION

#### 3.1 Before the reclamation projects

Before the four reclamation projects (Exp 0), during spring tide (Fig.6a), the surface RUWF in the North Channel, North Passage and South Passage flowed seaward. Because of the special topography of the North Branch, the RUWF in the North Branch flows landward (Chen et al., 2019). The NTWF and WDR in the North Branch are  $-288.78 \text{ m}^3/\text{s}$  and  $-2.52\%$  (shown in Table 4), respectively, where the negative sign indicates that the water is transported from the North Branch into the South Branch. This indicates that river runoff flows into the sea mainly through the South Branch, and most of the river runoff (63.41%) flows into the sea through the North Channel rather than the South Channel (Table 4). Similarly, the South Passage (53.24%) is the main channel for river runoff into the sea (Table 4). On eastern Chongming Island, the RUWF flows northward because of the action of tidal pumping transport and tidal Stokes transport (Qiu and Zhu, 2015). Additionally, in the South Branch, the RUWF is seaward, but the RUWF is smaller in the bottom layer because of the bottom friction (Fig.6b). The bottom RUWF near the river mouth is landward due to the strong salinity front (Yuan and Zhu, 2017). The RUWF in the north of the RP-EHS flows seaward, and that in the east of the RP-EHS flows landward. The distribution of RUSF (as shown in Fig.6 (c, d)) is similar to that of RUWF. The magnitude of the RUSF is much larger outside of the river mouth because of the high salinity in that area. The RUSF on the northern side of the North Passage flows landward, which brings highly saline water into the area around the mouth of the North Channel. The North Branch contains highly saline water due to the lower WDR (Table 4), and the SSO is simulated, which is the result of the RUWF and RUSF from the upper reaches of the North Branch flowing into

the South Branch. The low-salinity water around eastern Chongming Island extends northeastward (Fig.6 (e, f)). As a result, the saltwater intrusion is strongest in the South Passage and weakest in the North Channel in the Yangtze River Estuary, and the bottom saltwater intrusion is stronger than the surface.

**Table 4 NTWF and WDR in each outlet in the Yangtze River Estuary during spring and neap tides in different experiments (North Brach: NB, South Branch: SB, North Channel: NC, South Channel: SC, North Passage: NP, South Passage: SP)**

	NTWF/(m <sup>3</sup> /s)				WDR/(%)			
	Spring		Neap		Spring		Neap	
	NB	SB	NB	SB	NB	SB	NB	SB
Exp 0	-288.78	11 756.87	83.16	12 851.92	-2.52	102.52	0.64	99.36
Exp 1	-275.44	11 758.73	120.23	12 811.75	-2.40	102.4	0.93	99.07
Exp 2	-251.84	11 731.59	137.82	12 813.05	-2.19	102.19	1.06	98.94
Exp 3	-303.76	11 775.72	81.86	12 863.22	-2.65	102.65	0.63	99.37
Exp 4	-294.06	11 753.63	76.62	12 841.87	-2.57	102.57	0.59	99.41
Exp 5	-284.63	11 715.41	78.45	12 839.29	-2.49	102.49	0.61	99.39
	NC	SC	NC	SC	NC	SC	NC	SC
Exp 0	7 370.9	4 254.05	7 262.47	5 664.21	63.41	36.59	56.18	43.82
Exp 1	7 890.09	3 725.49	7 119.47	5 754.73	67.93	32.07	55.3	44.7
Exp 2	7 302.03	4 294.89	7 238.31	5 655.11	62.97	37.03	56.14	43.86
Exp 3	7 162.64	4 485.52	6 917.5	6 001.42	61.49	38.51	53.55	46.45
Exp 4	8 172.57	3 434.48	7 497.34	5 431.38	70.41	29.59	57.99	42.01
Exp 5	7 424.41	4 149.26	7 239.02	5 666.04	64.15	35.85	56.09	43.91
	NP	SP	NP	SP	NP	SP	NP	SP
Exp 0	2 263.57	2 576.97	5 218.9	1 426.46	46.76	53.24	78.53	21.47
Exp 1	1 875.71	1 938.86	5 241.24	1 327.91	49.17	50.83	79.79	20.21
Exp 2	2 292.63	2 619.52	5 202.37	1 431.38	46.67	53.33	78.42	21.58
Exp 3	2 290.92	2 441.62	5 403.97	1 486.16	48.41	51.59	78.43	21.57
Exp 4	1 561.98	2 409.88	5 078.89	1 343.38	39.33	60.67	79.08	20.92
Exp 5	2 461.38	2 214.94	5 267.11	1 315.79	52.63	47.37	80.01	19.99



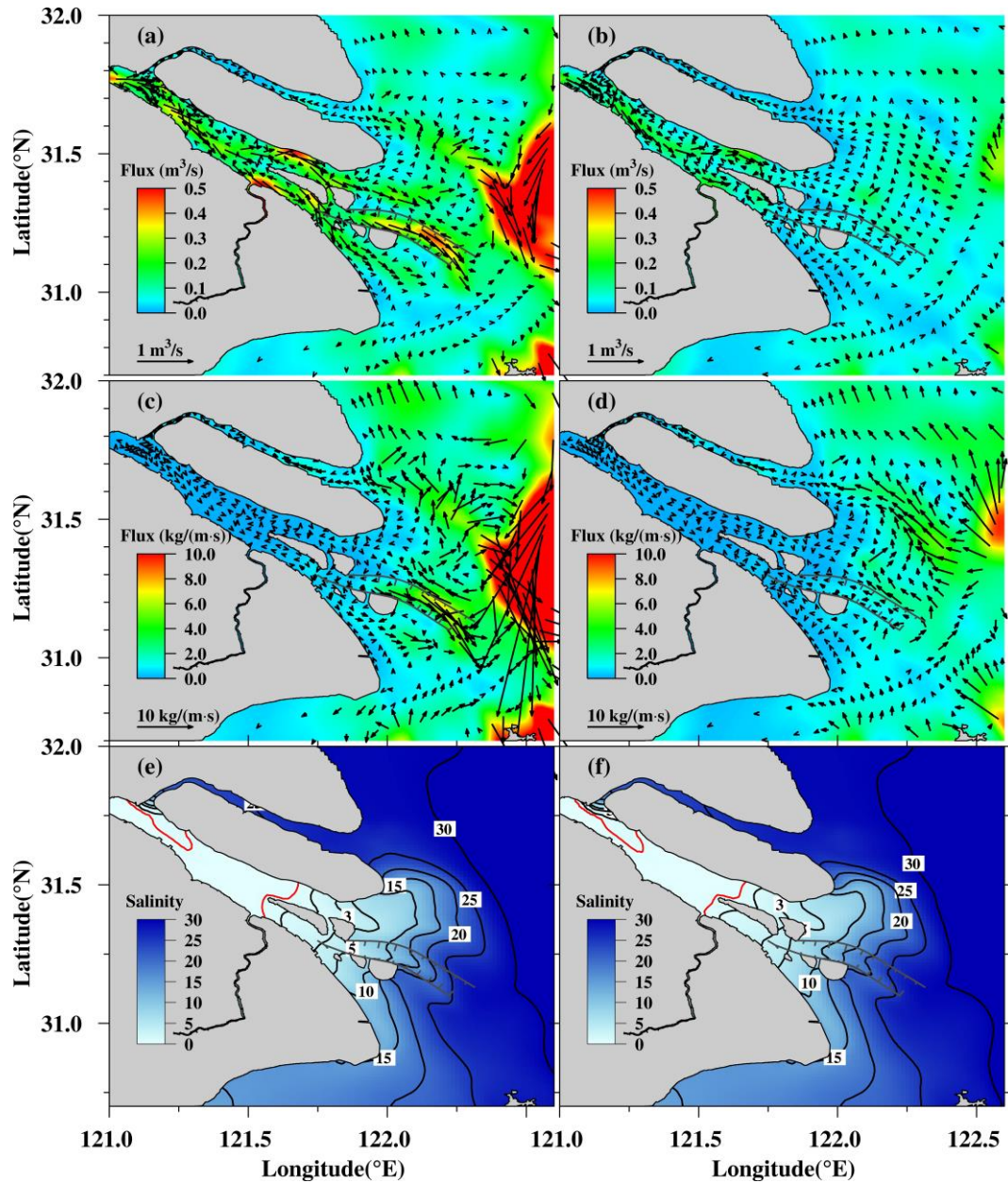


**Fig.6 Distributions of the RUWF (a, b), RUSF (c, d) and average salinity (e, f) in the surface (left) and bottom (right) layers during spring tide before the four reclamation projects. The red isohaline is 0.45, which is the salinity standard of drinking water**

During neap tide (Fig.7), wind is dominant because tides become weaker, and the RUWF and RUSF around the outside of the river mouth flow southward due to the effect of the northerly winter monsoon (Chen et al., 2019; Lyu and Zhu, 2019; Wu et al., 2014). In addition, the SSO disappeared, which is different from spring tide. The NTWF in the North Branch became a positive value ( $83.16 \text{ m}^3/\text{s}$ ), and the WDR was 0.64% (Table 4). The North Channel (56.18%) is the main channel for river discharge rather than the South Channel (Table 4). Because of the blockage of the stronger salinity front in the South Passage, the North Passage (78.53%) is the main channel for river discharge (Table 4). The bottom RUWF and RUSF near the river mouth flow landward due to a strong salinity front. Additionally, distinct saline wedges form around the river mouth due to weaker tidal mixing.



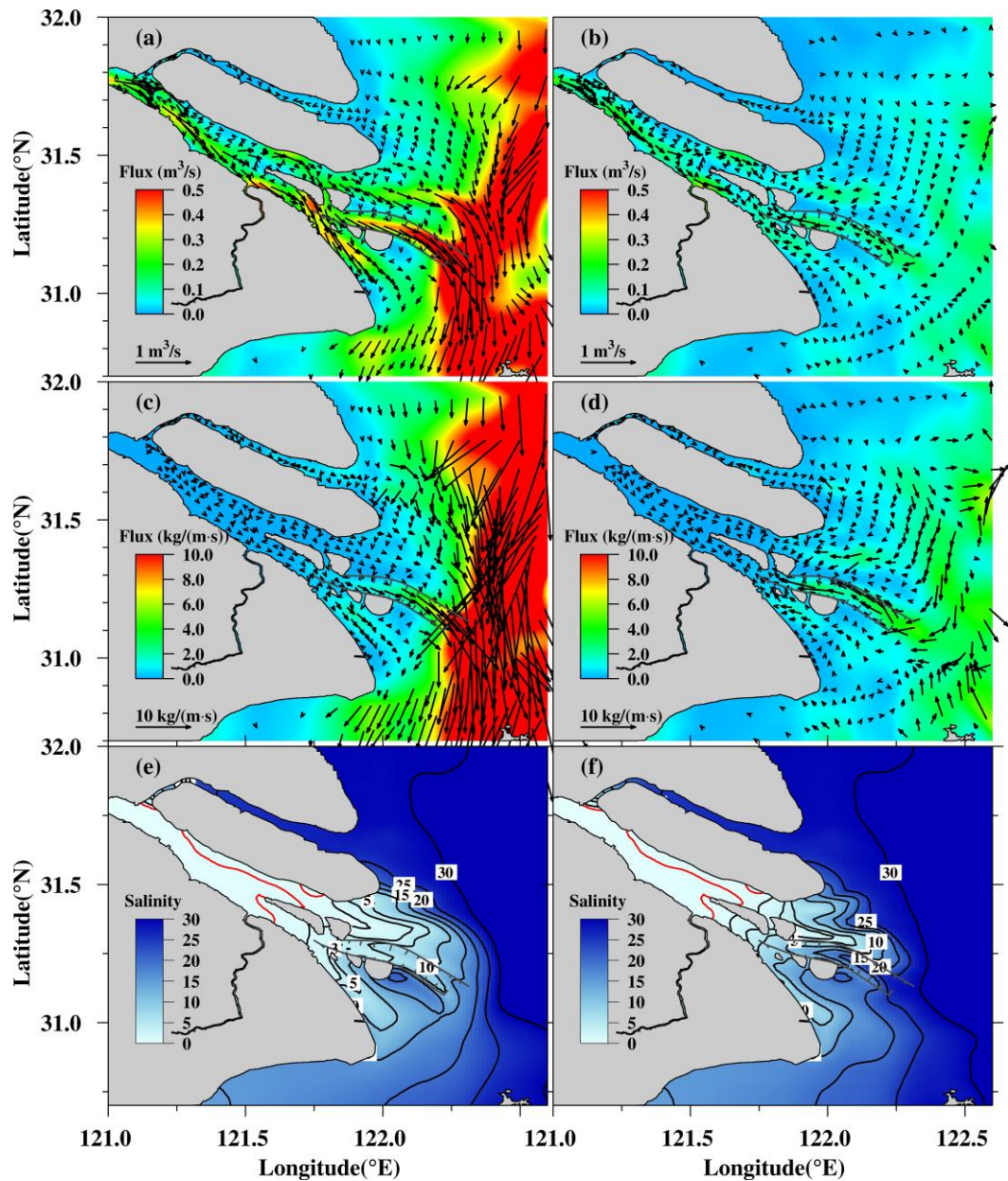
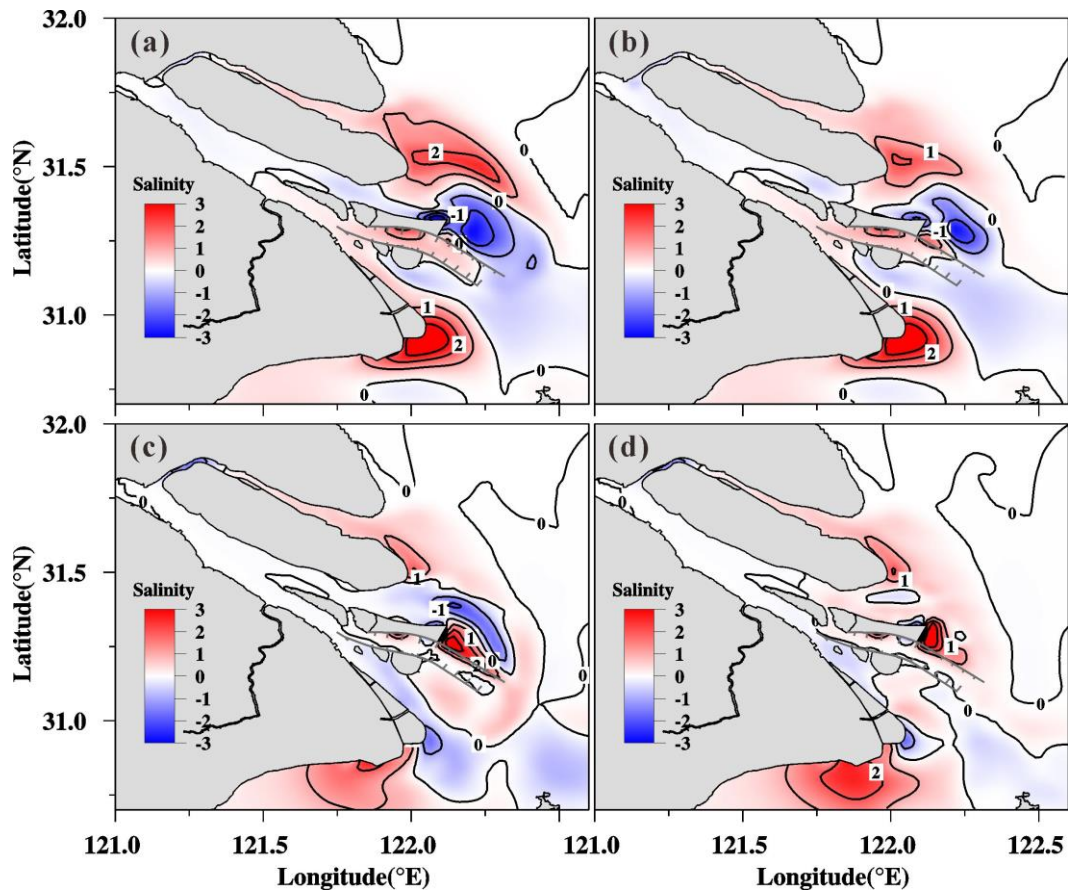


Fig.7 The same as Fig.6 except during neap tide

As shown by the above results, the four reclamation projects should have a strong influence on saltwater intrusion in the Yangtze River Estuary. To determine the reason and mechanism for the variation, the other four experiments (Exp 2-5) were performed. In this way, the effect of the individual reclamation project can be distinguished from the total effects of the four reclamation projects on saltwater intrusion.



**Fig.8 Differences in the salinity distributions in the surface (left) and bottom (right) layers during spring tide (a, b) and neap tide (c, d) after and before the four reclamation projects (Exp 1-Exp 0)**

### 3.2 After the reclamation projects

The difference in the average salinity distribution after completion of the four reclamation projects (Exp 1-Exp 0) is shown in Fig.8. During spring tide, the surface and bottom salinity in the upper reaches of the North Branch decreases by approximately 0.5. In contrast, the salinity in the middle and lower reaches of the North Branch increases by approximately 1.0. In the area east of Chongming Island, the salinity increases by more than 2.0. In the South Branch, the surface and bottom salinity decrease slightly. Therefore, the intensity of the SSO weakens after the four reclamation projects. In the North Channel, the salinity near the QCSR decreases slightly. However, the salinity in the area east of the RP-EHS decreases significantly. In particular, in the zone northeast of the RP-EHS, the maximum magnitude is above 2.0. In the South Channel, the salinity increases slightly. In the North Passage, the overall salinity increases by approximately 1.0. In the South Passage, the salinity variation presents a decreased distribution on the north side and increases on the south side. The maximum salinity variation area is located southeast of the RP-NHS, where it increases by more than 3.0.

Similarly, during neap tide (Fig.8 (c, d)), the salinity decreases in the upper reaches and increases in the

middle and lower reaches of the North Branch. The variation is approximately 1.0. The salinity east of Chongming Island also increases by approximately 1.0. The area of surface salinity decrease in the North Channel widens. However, the difference in the bottom salinity distribution varies differently from that during spring tide. The bottom salinity near the outlet of the North Channel increases by approximately 0.5. The surface and bottom salinities east of the RP-EHS can increase by more than 3.0, and they can change slightly in the North Passage. In the South Passage, the salinity variation is completely opposite to that during spring tide. South of the RP-NHS, salinity changes substantially by approximately 2.0.

### 3.3 Effects of every reclamation project

During spring tide, the effect of the RP-XCS narrows the transection in the middle reaches of the North Branch, induces the NTWF to increase by 36.94 m<sup>3</sup>/s and the WDR to increase by 0.33% (Table 5) and causes more freshwater to flow into the upper reaches of the North Branch from upstream, hindering landward saltwater intrusion in the lower reaches from the project and resulting in a salinity decrease in the upper reaches and a slight increase in the middle and lower reaches (Fig.9 (a, b)). The salinity decreases in the South Branch and increases east of Chongming Island and in the North Channel. Because the RP-XCS is small and located in the North Branch, the change in WDR is 0.44% in the bifurcation of the North Channel and South Channel and only 0.09% in the bifurcation of the North Passage and South Passage. The project's influence on the RUWF and RUSF has no obvious changes in the North Branch and South Branch (figures omitted due to space limitations).

**Table 5 The differences in the NTWF and WDR at each outlet in the Yangtze River Estuary during spring and neap tides before and after the reclamation project**

	NTWF/(m <sup>3</sup> /s)				WDR/(%)			
	Spring		Neap		Spring		Neap	
	NB	SB	NB	SB	NB	SB	NB	SB
$\Delta_{\text{Exp1-Exp0}}$	13.34	1.86	37.07	-40.17	0.12	-0.12	0.29	-0.29
$\Delta_{\text{Exp2-Exp0}}$	36.94	-25.28	54.66	-38.87	0.33	-0.33	0.42	-0.42
$\Delta_{\text{Exp3-Exp0}}$	-14.98	18.85	-1.3	11.3	-0.13	0.13	-0.01	0.01
$\Delta_{\text{Exp4-Exp0}}$	-5.28	-3.24	-6.54	-10.05	-0.05	0.05	-0.05	0.05
$\Delta_{\text{Exp5-Exp0}}$	4.15	-41.46	-4.71	-12.63	0.03	-0.03	-0.03	0.03
	NC	SC	NC	SC	NC	SC	NC	SC

$\Delta_{\text{Exp1-Exp0}}$	519.19	-528.56	-143	90.52	4.52	-4.52	-0.88	0.88
$\Delta_{\text{Exp2-Exp0}}$	-68.87	40.84	-24.16	-9.1	-0.44	0.44	-0.04	0.04
$\Delta_{\text{Exp3-Exp0}}$	-208.26	231.47	-344.97	337.21	-1.92	1.92	-2.63	2.63
$\Delta_{\text{Exp4-Exp0}}$	801.67	-819.57	234.87	-232.83	7	-7	1.81	-1.81
$\Delta_{\text{Exp5-Exp0}}$	53.51	-104.79	-23.45	1.83	0.74	-0.74	-0.09	0.09
	NP	SP	NP	SP	NP	SP	NP	SP
$\Delta_{\text{Exp1-Exp0}}$	-387.86	-638.11	22.34	-98.55	2.41	-2.41	1.26	-1.26
$\Delta_{\text{Exp2-Exp0}}$	29.06	42.55	-16.53	4.92	-0.09	0.09	-0.11	0.11
$\Delta_{\text{Exp3-Exp0}}$	27.35	-135.35	185.07	59.7	1.65	-1.65	-0.1	0.1
$\Delta_{\text{Exp4-Exp0}}$	-701.59	-167.09	-140.01	-83.08	-7.43	7.43	0.55	-0.55
$\Delta_{\text{Exp5-Exp0}}$	197.81	-362.03	48.21	-110.67	5.87	-5.87	1.48	-1.48

290

291       The effect of the RP-QCS narrows the upper reaches of the North Channel, causing the NTWF and WDR to  
292 decrease by 208.26 m<sup>3</sup>/s and 1.92% in the North Channel (Table 5), respectively, resulting in salinity increases in  
293 the North Channel and east of Chongming Island. This effect does not occur in the area north of the North Passage,  
294 as the salinity decreases in that area. The impact of the RP-QCS on the WDR change is 0.13% in the bifurcation  
295 of the North and South Branch and 1.65% in the bifurcation of the North Passage and South Passage. The salinity  
296 decreases slightly in the South Channel, North Passage and South Passage (Fig.9 (c, d)). The difference between  
297 the surface and bottom RUWF is landward near the QCSR after the RP-QCS, meaning that the seaward RUWF  
298 decreases.

299       Among the effects of the RP-EHS, the NTWF and WDR increased by 801.67 m<sup>3</sup>/s and 7.0% in the North  
300 Channel (Table 5), respectively, meaning that more freshwater was bifurcated into the North Channel, resulting in  
301 salinity decreases of 1-2 in the mouth of the North Channel. The other reason for the salinity decrease is that the  
302 RP-EHS lengthens the North Channel seaward. The differences in the RUWF and RUSF in the area east of  
303 Chongming Island are the opposite of the directions before the RP-EHS, meaning that the southward transport of  
304 water and salt by the northerly wind is weakened by the RP-EHS, inducing the highly saline water to gather in the  
305 area east of Chongming Island, resulting in salinity increases of approximately 0.5 in that area. In the South  
306 Channel, the NTWF and WDR decreased by 819.57 m<sup>3</sup>/s and 7.0%, respectively, after the RP-EHS, which led the  
307 NTWF in the North and South Passages to decrease by 701.59 and 167.09 m<sup>3</sup>/s, respectively. For this reason, the  
308 salinity in the South Channel increased by approximately 1.0 after the projects. In the North Passage, the WDR  
309 decreased by 7.43%, resulting in a surface and bottom salinity increase of 1.0. The reason for the salinity increase

310 in the North Passage is that the project blocks the lower salinity water flowing southward in the North Channel  
311 into the North Passage, which is forced by the northerly wind and Coriolis force.

312 Among the effects of the RP-NHS, the NTWF and WDR in the South Passage decreased by 362.03 m<sup>3</sup>/s and  
313 5.87% (Table 5), respectively, because the transect area at the entrance of the South Passage was narrowed. The  
314 impact of the RP-NHS on the WDR change is only 0.03% in the bifurcation of the North Branch and South  
315 Branch and 0.74% in the bifurcation of the North Channel and South Channel. The narrower transect area reduces  
316 the landward salt flux, resulting in a salinity decrease in the South Passage, even though the WDR in the South  
317 Passage decreases. In the southeastern area of the project, the salinity increases by more than 3.0 because the  
318 RP-NHS blocks the upstream river water flowing there and gathers highly saline water from the open sea.

319 Comparing the distribution of the salinity difference between Exp 1 and Exp 0 (Fig.8 (a, b)), with and  
320 without the individual reclamation projects (Exp 2, Fig.9 (a, b); Exp 3, Fig.9 (c, d); Exp 4, Fig.9 (e, f) and Exp 5,  
321 Fig.9 (g, h)), the salinity decrease in the upper reaches of the North Branch and increases in the middle and lower  
322 reaches of the North Branch are mainly caused by the RP-XCS. The salinity decrease in the North Channel is  
323 caused by the RP-EHS, and the effect is much larger than the effect of the RP-QCS, which increases the salinity.  
324 The salinity decrease in the South Passage is caused by the RP-NHS, and the effect is much larger than the effect  
325 of the RP-EHS, which increases the salinity in that area. A distinct salinity increase southeast of the RP-NHS is  
326 completely induced by the RP-NHS. In the area east of Chongming Island, the salinity increase is considerable  
327 under the cumulative effect of the four reclamation projects, where the RP-EHS has the largest contribution, the  
328 RP-QCS has the second largest contribution, the RP-XCS has the third largest contribution, and the RP-NHS has a  
329 very small negative contribution.



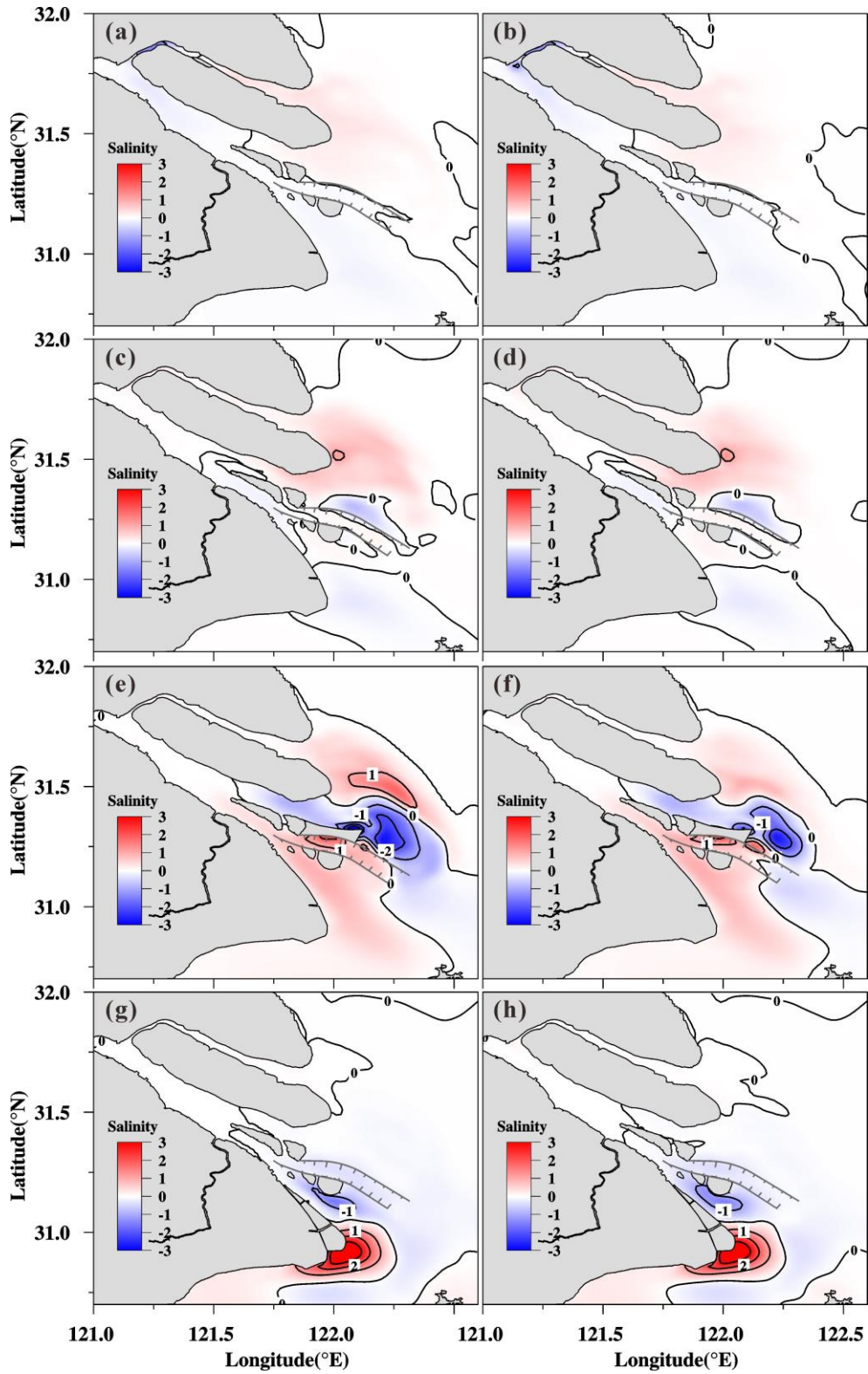


**Fig.9 Differences in salinity distributions in the surface (left) and bottom (right) layers during spring tide after and before RP-XCS (a, b), RP-QCS (c, d), RP-EHS (e, f), and RP-NHS (g, h)**

During neap tide, the RP-XCS caused the NTWF to increase by 54.66 m<sup>3</sup>/s and the WDR to increase by 0.42% (Table 5), resulting in a salinity change in the North Branch that is similar to that during spring tide, with a decrease in the upper reaches and an increase in the middle and lower reaches (Fig.10 (a, b)). Salinity increases east of Chongming Island and in the North Channel. The RP-XCS changes the WDR by only 0.04% in the

337 bifurcation of the North Channel and South Channel and 0.11% in the bifurcation of the North Passage and South  
338 Passage because the project is located far away.

339 The RP-QCS caused the NTWF and WDR to decrease by 344.21 m<sup>3</sup>/s and 2.63% in the North Channel  
340 (Table 5), respectively, resulting in salinity increases in the North Channel, in the area east of Chongming Island,  
341 and in the lower reaches of the North Branch. The impact of the RP-QCS on the WDR change was 0.01% in the  
342 bifurcation of the North and South Branch and 1.10% in the bifurcation of the North and South Passage. The  
343 salinity increased slightly in the South Channel, North Passage and South Passage (Fig.10 (c, d)).

344 The RP-EHS resulted in increases in the NTWF and WDR by 234.87 m<sup>3</sup>/s and 1.81% in the North Channel  
345 (Table 5), respectively, meaning that more freshwater is bifurcated into the North Channel, resulting in a salinity  
346 decrease of more than 1.0 in the mouth of the North Channel. In the South Channel, the NTWF and WDR  
347 decreased by 234.87 m<sup>3</sup>/s and 1.81%, respectively, after the RP-EHS, which caused the NTWF in the North  
348 Passage and the South Passage to decrease by 104.01 and 83.08 m<sup>3</sup>/s, respectively. The salinities in the South  
349 Channel, North Passage and South Passage increased by 0.5-1.0. The salinity in the area east of the RP-EHS  
350 increased for the same reason as during spring tide described above.

351 The RP-NHS caused the NTWF and WDR in the South Passage to decrease by 5.87 m<sup>3</sup>/s and 1.48% (Table  
352 5), respectively. However, the salinity in the South Passage decreased by 0.5 to 1.0 even though the WDR in the  
353 South Passage decreased because the RP-NHS narrowed the entrance of the South Passage, which reduced the  
354 landward salt flux from the open sea. The impact of the RP-NHS on the WDR change was only 0.03% in the  
355 bifurcation of the North Branch and South Branch and 0.09% in the bifurcation of the North Channel and South  
356 Channel. In the southern area of the RP-NHS, the salinity increased by more than 2.0, and the cause was the same  
357 as that during spring tide.

358 Comparing the difference in salinity distributions between Exp 1 and Exp 0 (Fig.8 (c, d)), with and without  
359 the individual reclamation project (Exp 2, Fig.10 (a, b); Exp 3, Fig.10 (c, d); Exp 4, Fig.10 (e, f) and Exp 5, Fig.10  
360 (g, h)), the salinity decreases in the upper reaches of the North Branch and increases in the middle and lower  
361 reaches of the North Branch are mainly caused by the RP-XCS. The salinity decrease in the North Channel is  
362 caused by the RP-EHS, and the effect is much larger than the effect of the RP-QCS, which increases the salinity.  
363 The salinity decrease in the South Passage is caused by the RP-NHS, and the effect is much larger than the effect  
364 of the RP-EHS, which caused the salinity to increase in that area. A distinct salinity increase south of the RP-NHS  
365 was induced by the RP-NHS. In the area east of Chongming Island, the salinity increase was caused by the  
366 cumulative effect of the RP-QCS and RP-NHS.

367



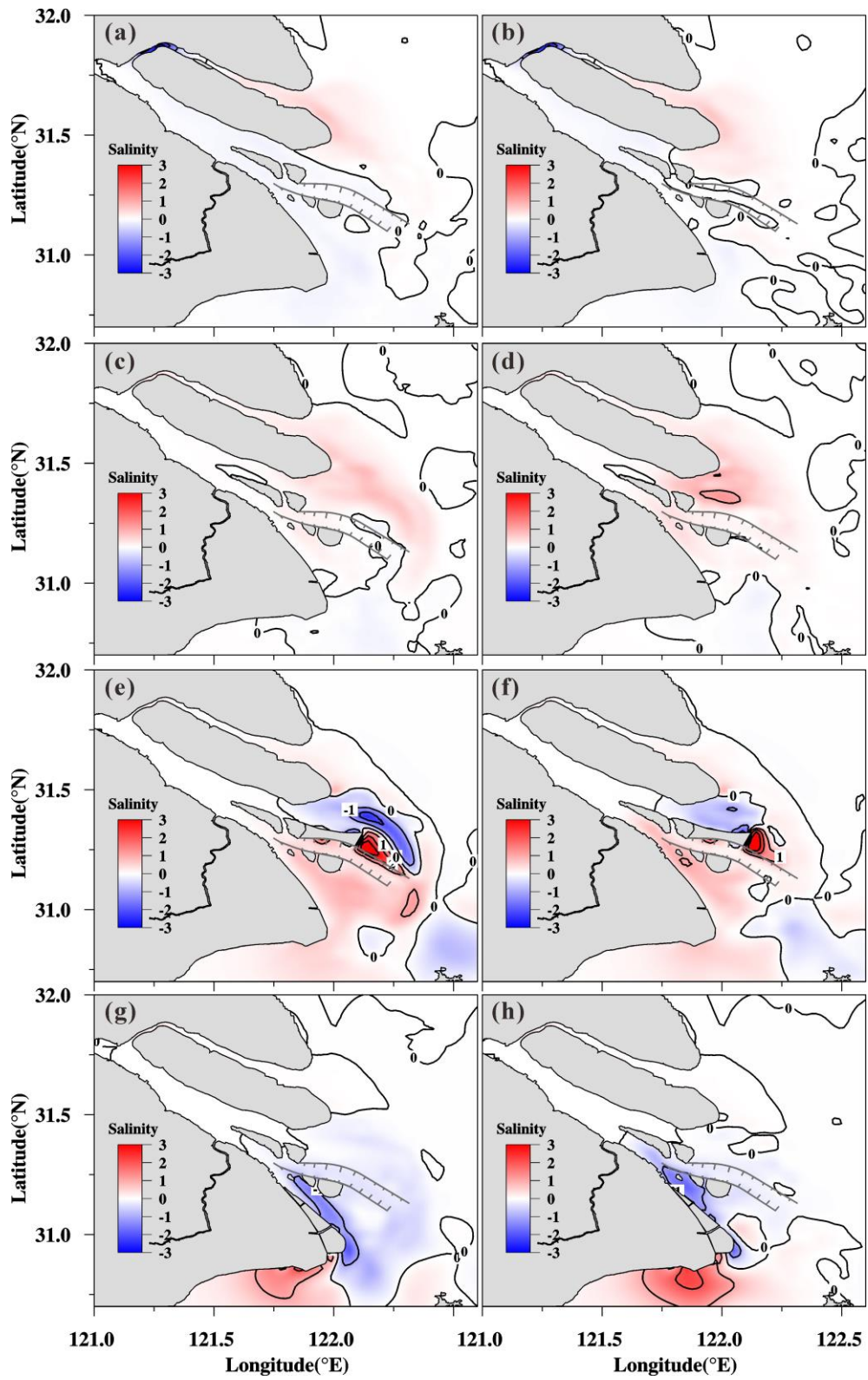
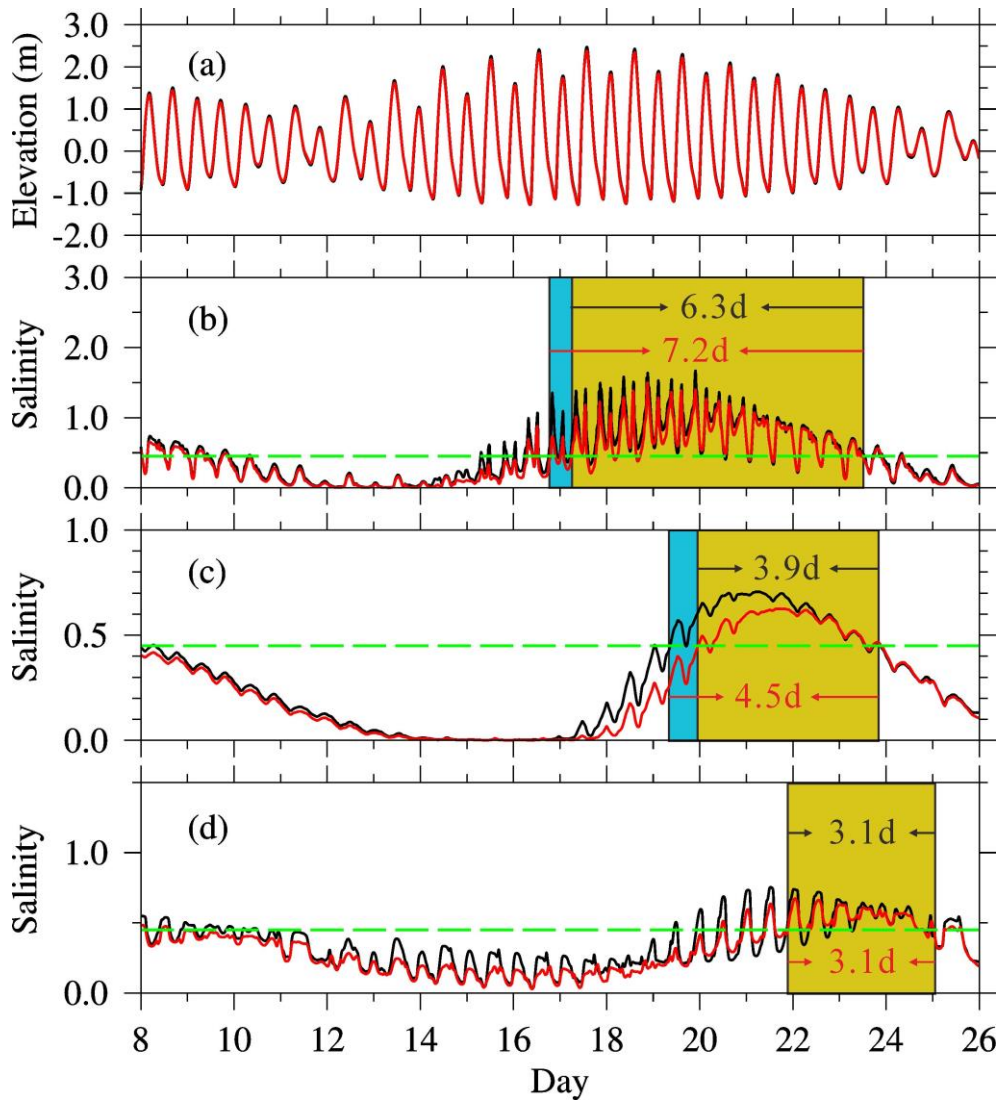


Fig.10 The same as Fig.9 except during neap tide



**Fig.11 Simulated temporal variation in elevation at the water intake of the QCSR (a) and the salinity at the water intakes of the DFXSR (b), CHR (c) and QCSR (d) before (black lines) and after (red lines) the four reclamation projects from February 8 to February 26, 2015. The green line is 0.45. The blue and yellow belts indicate the longest continuous non-suitable water intake periods for the reservoirs before and after the four reclamation projects, respectively**

### 3.4 Effects on reservoirs

Due to the low river discharge in winter, saltwater intrusion frequently threatens freshwater intake from the Yangtze River Estuary. Previous studies indicated that the salinity at the QCSR is controlled by the SSO and saltwater intrusion along the North Channel. However, the salinity at the CHR and DFXSR is completely influenced by the SSO (Chen and Zhu, 2014; Li et al., 2014). The temporal salinity variations at the water intakes of the QCSR, CHR and DFXSR before and after the four reclamation projects are shown in Fig.11, and the corresponding tidally averaged salinities are shown in Table 6. As demonstrated in previous studies, the reservoir still cannot receive water if the duration of salinity lower than 0.45 is shorter than 4.0 hours (Zhu et al., 2013).

Therefore, the reservoir still cannot intake water during the flood and ebb periods, even though the salinity will be below 0.45 over less than 4.0 hours. As mentioned above, the SSOs are somewhat weakened after the four reclamation projects. The saline water that threatened the reservoirs is mainly from the SSO. The longest continuous nonsuitable water intake period for the QCSR, CHR and DFXSR slightly decreased overall (Fig.11 (b, c, d)). The longest continuous nonsuitable water intake period for the DFXSR decreased from 7.2 days to 6.3 days, that for the CHR decreased from 4.5 days to 3.9 days, and that for the QCSR was still 3.1 days even though the average salinity decreased. Correspondingly, during spring tide, moderate tide after spring tide (MTST), neap tide, and moderate tide after neap tide (MTNT), the tidally averaged salinity reductions at the water intakes of the DFXSR, CHR and QCSR are 0.16, 0.04, and 0.03 and 0.08, 0.08, 0.10, 0.02 and 0.00, and 0.06, 0.02, 0.04 and 0.06, respectively. These findings indicate that the four reclamation projects favor the security of freshwater resources in the Yangtze River Estuary.

**Table 6 Tidally averaged salinity and difference during spring tide, MTST, neap tide and MTNT at the water intakes of the DFXSR, CHR and QCSR before and after the four reclamation projects**

		Spring	MTST	Neap	MTNT
DFXSR	Exp 0	0.81	0.86	0.13	0.20
	Exp 1	0.65	0.82	0.10	0.12
	$\Delta_{\text{Exp1-Exp0}}$	-0.16	-0.04	-0.03	-0.08
CHR	Exp 0	0.16	0.64	0.14	0.01
	Exp 1	0.08	0.54	0.12	0.01
	$\Delta_{\text{Exp1-Exp0}}$	-0.08	-0.10	-0.02	0.00
QCSR	Exp 0	0.21	0.48	0.32	0.20
	Exp 1	0.15	0.46	0.28	0.14
	$\Delta_{\text{Exp1-Exp0}}$	-0.06	-0.02	-0.04	-0.06

400

## 401 4 CONCLUSIONS

402 The effects of the four reclamation projects and each individual project on the saltwater intrusion and water  
403 resources in the Yangtze River Estuary were simulated by a 3D numerical model. The results of the study show  
404 that for a multichannel estuary, a local reclamation project changes the local topography, changes the WDR  
405 between channels, and influences the water and salt transport in the estuary. The cumulative effects of the four  
406 reclamation projects on saltwater intrusion in the North Branch and South Branch, the North Channel and South

407 Channel, and in the North Passage and South Passage, in spring tide and neap tide, are different, and their causes  
408 were analyzed in detail.

409 The SSO was somewhat weakened after the completion of the four reclamation projects, which resulted in  
410 slight salinity decreases at the water intakes of the DFXSR, CHR and QCSR. The cumulative effects of the four  
411 reclamation projects are favorable for the security of freshwater resources in the Yangtze River Estuary.

412 The conclusions from this study are only appropriate for saltwater intrusion under mean climate conditions in  
413 the dry season in the Yangtze River Estuary. As mentioned in the description of the model configuration, all of the  
414 numerical experiments were run under the mean runoff and wind conditions. Thus, the results cannot reflect the  
415 impacts of the projects on saltwater intrusion in the Yangtze River Estuary under extreme weather conditions.

416

## 417 **5 DATA AVAILABILITY STATEMENT**

418 The observation and model data and computer codes used in this paper are available from the authors (e-mail:  
419 jrzhu@sklec.ecnu.edu.cn).

420

## 421 **6 ACKNOWLEDGMENT**

422 This work was supported by the National Natural Science Foundation of China (41476077, 41676083) and  
423 Shanghai Institute of Eco-Chongming. We are grateful for the support from the CSC (China Scholarship Council).

424

## 425 **References**

426 Andrews S W, Gross E S, Hutton P H. 2017. Modeling salt intrusion in the San Francisco Estuary prior to anthropogenic influence.  
427 Continental Shelf Research, 146: 58-81, <https://doi.org/10.1016/j.csr.2017.07.010>.

428 Birch G F, Murray O, Johnson I et al. 2009. Reclamation in Sydney estuary, 1788-2002. Australian Geographer, 40(3): 347-368,  
429 <https://doi.org/10.1080/00049180903127788>.

430 Blumberg A F. 1994. A primer for ECOM-si. Technical report of HydroQual, 6p.

431 Buggy C J, Tobin J M. 2006. Spatial distribution of nine metals in surface sediment of an urban estuary prior to a large scale  
432 reclamation project. Marine Pollution Bulletin, 8(52): 969-974, <https://doi.org/10.1016/j.marpolbul.2006.04.006>.

433 Chen C S, Zhu J R, Ralph E et al. 2001. Prognostic modeling studies of the Keweenaw current in Lake Superior. Part I: Formation  
434 and evolution. Journal of Physical Oceanography, 31(2): 379-395,  
435 [https://doi.org/10.1175/1520-0485\(2001\)031<0379:PMSOTK>2.0.CO;2](https://doi.org/10.1175/1520-0485(2001)031<0379:PMSOTK>2.0.CO;2).

436 Chen J, Zhu J R. 2014. Sources for saltwater intrusion at the water intake of Qingcaosha Reservoir in the Changjiang Estuary.  
437 Haiyang Xuebao, 36(11): 131-141. (in Chinese)

438 Chen J, Zhu J R. 2014. Impacts of the reclamation project of Xincunsha on the saltwater intrusion in the North Branch of the  
439 Changjiang Estuary. Journal of East China Normal University (Natural Science), 4: 163-172. (in Chinese)

440 Chen Q, Zhu J R, Lyu H H et al. 2019. Determining Critical River Discharge as a Means to Provide Water Supply Security to the  
441 Changjiang River Estuary, China. Journal of Coastal Research, 35(5): 1 087-1 094,  
442 <https://doi.org/10.2112/JCOASTRES-D-18-00165.1>.

443 Chua T. 1993. Essential elements of integrated coastal zone management. Ocean and Coastal Management, 21(1-3): 81-108,  
444 [https://doi.org/10.1016/0964-5691\(93\)90021-P](https://doi.org/10.1016/0964-5691(93)90021-P).

445 Doornbos G, Groenendijk A M, Jo Y W. 1986. Nakdong estuary barrage and reclamation project: preliminary results of the botanical,  
446 macrozoobenthic and ornithological studies. Biological Conservation, 38(2): 115-142,  
447 [https://doi.org/10.1016/0006-3207\(86\)90069-8](https://doi.org/10.1016/0006-3207(86)90069-8).

448 Editorial Board for Marine Atlas. 1992. Ocean Atlas in Huanghai Sea and East China Sea (Hydrology), Beijing: China Ocean Press,  
449 China.1p.

450 Fofonoff P, Millard Jr R C. 1983. Algorithms for computation of fundamental properties of seawater. Unesco Technical Papers in  
451 Marine Sciences, 44: 53, <http://hdl.handle.net/11329/109>.

452 Fu Y B, Cao K, Wang F et al. 2010. Primary quantitative evaluation method on sea enclosing and land reclamation strength and  
453 potential. Ocean Development and Management, 1(27): 1-30. (in Chinese)

454 Geyer W R. 1993. The importance of suppression of turbulence by stratification on the estuarine turbidity maximum. Estuaries and  
455 Coasts, 16(1): 113-125, <https://doi.org/10.2307/1352769>.

456 Han Z C, Pan C H, Yu J et al. 2001. Effect of large-scale reservoir and river regulation/reclamation on saltwater intrusion in Qiantang  
457 Estuary. Science in China Series B: Chemistry, 44(s1): 221-229, <https://doi.org/10.1007/BF02884830>.

458 Kantha L H, Clayson C A. 1994. An improved mixed layer model for geophysical applications. Journal of Geophysical Research:  
459 Oceans, 99(C12): 25235-25266, <https://doi.org/10.1029/94JC02257>.

460 Kuijpers J W M. 1995. Ecological restoration of the Rhine/Maas estuary. Water Science and Technology, 31(8): 187-195,  
461 [https://doi.org/10.1016/0273-1223\(95\)00370-3](https://doi.org/10.1016/0273-1223(95)00370-3).

462 Lax P D, Wendroff B. 1962. On the stability of difference schemes. Communications on pure and applied mathematics, 15(4):  
463 363-371, <https://doi.org/10.1002/cpa.3160150401>.

464 Li L J, Zhu J R. 2015. Impacts of the reclamation project of Nanhui tidal flat on currents and saltwater intrusion in the Changjiang  
465 Estuary. Journal of East China Normal University (Natural Science), 4: 77-86. (in Chinese)

466 Li L, Zhu J R, Wu H. 2012. Impacts of wind stress on saltwater intrusion in the Yangtze Estuary. Science China Earth Sciences, 55(7):

1 178-1 192, <https://doi.org/10.1007/s11430-011-4311-1>.

Li L, Zhu J R, Wu H et al. 2014. Lateral saltwater intrusion in the North Channel of the Changjiang Estuary. *Estuaries and Coasts*, 37(1): 36-55, <https://doi.org/10.1007/s12237-013-9669-1>.

Li L, Zhu J R, Wu H et al. 2010. A numerical study on water diversion ratio of the Changjiang (Yangtze) estuary in dry season. *Chinese Journal of Oceanology and Limnology*, 28(3): 700-712, <https://doi.org/10.1007/s00343-010-9114-2>.

Lyu H H, Zhu J R. 2018. Impact of the bottom drag coefficient on saltwater intrusion in the extremely shallow estuary. *Journal of Hydrology*, 557: 838-850, <https://doi.org/10.1016/j.jhydrol.2018.01.010>.

Lyu H H, Zhu J R. 2019. Impacts of Tidal flat reclamation on saltwater intrusion and freshwater resources in the Changjiang Estuary. *Journal of Coastal Research*, 35(2): 314-321, <https://doi.org/10.2112/JCOASTRES-D-18-00077.1>.

Ma Y, Rong K, Mangalagu D et al. 2018. Co-evolution between urban sustainability and business ecosystem innovation: Evidence from the sharing mobility sector in Shanghai. *Journal of Cleaner Production*, 188: 942-953, <https://doi.org/10.1016/j.jclepro.2018.03.323>.

Manda A, Matsuoka K. 2006. Changes in tidal currents in the Ariake Sound due to reclamation. *Estuaries and Coasts*, 29(4): 645-652, <https://doi.org/10.1007/BF02784289>.

Mellor G L, Yamada T. 1982. Development of a turbulence closure model for geophysical fluid problems. *Reviews of Geophysics*, 20(4): 851-875, <http://dx.doi.org/10.1029/RG020i004p00851>.

Nichols F H, Cloern J E, Luoma S N, et al. 1986. The modification of an estuary. *Science*, 231(4738): 567-573, <https://doi.org/10.1126/science.231.4738.567>.

Qiu C, Zhu J R. 2013. Influence of seasonal runoff regulation by the Three Gorges Reservoir on saltwater intrusion in the Changjiang River Estuary. *Continental Shelf Research*, 71: 16-26, <https://doi.org/10.1016/j.csr.2013.09.024>.

Qiu C, Zhu J R. 2015. Assessing the influence of sea level rise on salt transport processes and estuarine circulation in the Changjiang River estuary. *Journal of Coastal Research*, 31(3): 661-670, <https://doi.org/10.2112/JCOASTRES-D-13-00138.1>.

Qiu Cheng, Zhu Jianrong, Gu Yuliang. 2012. Impact of seasonal tide variation on saltwater intrusion in the Changjiang River estuary. *Chinese Journal of Oceanology and Limnology*, 30(2): 342-351, <https://doi.org/10.1007/s00343-012-1115-x>.

Shen H T, Mao Z C, Zhu J R. 2003. *Saltwater Intrusion in the Changjiang Estuary*. Beijing: China Ocean, 175p. (in Chinese)

Shi C, Hutchinson S M, Yu L et al. 2001. Towards a sustainable coast: an integrated coastal zone management framework for Shanghai, People's Republic of China. *Ocean and Coastal Management*, 44(5-6): 411-427, [https://doi.org/10.1016/S0964-5691\(01\)00058-8](https://doi.org/10.1016/S0964-5691(01)00058-8).

Simpson J H, Brown J, Matthews J et al. 1990. Tidal straining, density currents, and stirring in the control of estuarine stratification. *Estuaries*, 13(2): 125-132, <https://doi.org/10.2307/1351581>.

Song D, Wang X H, Zhu X et al. 2013. Modeling studies of the far-field effects of tidal flat reclamation on tidal dynamics in the East

498 China Seas. *Estuarine Coastal & Shelf Science*, 133(4): 147-160, <https://doi.org/10.1016/j.ecss.2013.08.023>.

499 Van M D S, Oost A P, Wang Z B et al. 2016. The effect of land reclamations and sediment extraction on the suspended sediment  
500 concentration in the Ems Estuary. *Marine Geology*, 376: 147-157, <https://doi.org/10.1016/j.margeo.2016.03.007>.

501 Wang S X, Zhu J R. 2015. Saltwater intrusion sources at the water intake of Qingcaosha reservoir in different tidal pattern and wind  
502 case. *Journal of East China Normal University (Natural Science)*, 4: 65-76. (in Chinese)

503 Wang W, Liu H, Li Y Q et al. 2014. Development and management of land reclamation in China. *Ocean and Coastal Management*,  
504 102: 415-425, <https://doi.org/10.1016/j.ocecoaman.2014.03.009>.

505 Willmott C J. 1981. On the validation of models. *Physical Geography*, 2(2): 184-194,  
506 <https://dx.doi.org/10.1080/02723646.1981.10642213>.

507 Wu H, Zhu J R. 2010. Advection scheme with 3rd high-order spatial interpolation at the middle temporal level and its application to  
508 saltwater intrusion in the Changjiang Estuary. *Ocean Modelling*, 33(1): 33-51, <https://doi.org/10.1016/j.ocemod.2009.12.001>.

509 Wu H, Zhu J R, Shen J et al. 2011. Tidal modulation on the Changjiang River plume in summer. *Journal of Geophysical Research:*  
510 *Atmospheres*, 116(C8): 192-197, <https://dx.doi.org/10.1029/2011JC007209>.

511 Wu H, Shen J, Zhu J R et al. 2014. Characteristics of the Changjiang plume and its extension along the Jiangsu Coast. *Continental*  
512 *Shelf Research*, 76(2): 108-123, <https://doi.org/10.1016/j.csr.2014.01.007>.

513 Wu H, Zhu J R, Chen B R et al. 2006. Quantitative relationship of runoff and tide to saltwater spilling over from the North Branch in  
514 the Changjiang Estuary: A numerical study. *Estuarine Coastal and Shelf Science*, 69(1-2): 125-132,  
515 <https://doi.org/10.1016/j.ecss.2006.04.009>.

516 Xu, T. 2014. Study on hydrodynamics and salinity environment after a large-scale reclamation project in the Oujiang River Estuary.  
517 *Modeling and Computation in Engineering III*, 17p, <https://doi.org/10.1201/b17064-4>.

518 Xue P F, Chen C S, Ding P X et al. 2009. Saltwater intrusion into the Changjiang River: A model-guided mechanism study. *Journal of*  
519 *Geophysical Research: Oceans*, 114(C2), <https://doi.org/10.1029/2008JC004831>.

520 Yuan R, Zhu J R. 2017. The Effects of dredging on Tidal Range and Saltwater Intrusion in the Pearl River Estuary. *Journal of Coastal*  
521 *Research*, 31(6): 1 357-1 362, <https://doi.org/10.2112/JCOASTRES-D-14-00224.1>.

522 Zheng L Y, Chen C S, Liu H D. 2003. A modeling study of the Satilla River Estuary, Georgia. i: flooding-drying process and water  
523 exchange over the salt marsh-estuary-shelf complex. *Estuaries*, 26(3): 651-669, <https://doi.org/10.1007/BF02711977>.

524 Zheng L Y, Chen C S, Zhang F Y. 2004. Development of water quality model in the Satilla River Estuary, Georgia. *Ecological*  
525 *Modelling*, 178(3): 457-482, <https://doi.org/10.1016/j.ecolmodel.2004.01.016>.

526 Zhu J R, 2003. Ocean numerical calculation method and numerical model. Beijing: China Ocean Press, China. p. 110-160. (in  
527 Chinese)

528 Zhu J R, Gu Y L, Wu H. 2013. Determination of the period not suitable for taking domestic water supply to the Qingcaosha reservoir



- 529 near Changjiang River Estuary. *Oceanologia et Limnologia Sinica*, 44(5): 1138-1145. (in Chinese)
- 530 Zhu J R, Wu H, Li L. 2015. Hydrodynamics of the Changjiang Estuary and Adjacent Seas. In: Zhang J ed. *Ecological Continuum*
- 531 from the Changjiang (Yangtze River) Watersheds to the East China Sea Continental Margin. Springer, Switzerland. p. 19-46.
- 532 Zhu J R, Wu H, Li L et al. 2010. Saltwater intrusion in the Changjiang Estuary in the extremely drought hydrological year 2006.
- 533 *Journal of East China Normal University (Natural Science)*, 4(1): 1-6. (in Chinese)